New Journal of Physics
The open-access journal for physics

On the triggering of the Ultimate Regime of convection

P-E Roche[1], **F Gauthier, R Kaiser and J Salort**
Institut Néel, CNRS/UJF, BP 166, F-38042 Grenoble cedex 9, France

New Journal of Physics **12** (2010) 085014 (26pp)
Received 9 February 2010
Published 26 August 2010
Online at http://www.njp.org/
doi:10.1088/1367-2630/12/8/085014

Abstract. Rayleigh–Bénard cells are one of the simplest systems for exploring the laws of natural convection in the highly turbulent limit. However, at very high Rayleigh numbers ($Ra \gtrsim 10^{12}$) and for Prandtl numbers of the order of one, experiments fall into two categories: some evidence a steep enhancement of the heat transfer while others do not. The origin of this apparent disagreement is at present still unexplained. This puzzling situation motivated a systematic study of the triggering of the regime with an enhanced heat transfer, originally named the 'Ultimate Regime' of convection. High-accuracy heat transfer measurements have been conducted in convection cells with various aspect ratios and different specificities, such as altered boundary conditions or obstacles inserted in the flow. The two control parameters, the Rayleigh and Prandtl numbers, have been varied independently to disentangle their relative influence. Among other results, it is found that (i) most experiments reaching very high Ra are not in disagreement if small differences in Prandtl number are taken into account, (ii) the transition is not directly triggered by the large-scale circulation present in the cell and (iii) the sidewalls of the cell have a significant influence on the transition. The characteristics of this Ultimate Regime are summarized and compared with the R Kraichnan prediction for the asymptotic regime of convection.

[1] Author to whom any correspondence should be addressed.

Contents

1. Introduction: an elusive regime **2**
1.1. An historical perspective 2
1.2. Motivation and organization of the paper 6
2. New very-high-resolution cryogenic He experiments **6**
3. The Grenoble regime and the Prandtl number **8**
3.1. Grenoble regime in the Ra–Pr parameter space 9
3.2. Prandlt number dependence of the Grenoble regime 11
4. The Grenoble regime and the Large-Scale Circulation (LSC) **12**
4.1. Is the wind changing when the transition occurs? 12
4.2. Is the transition altered by modifications of the LSC? 14
5. The Grenoble regime and sidewall **16**
5.1. Is the transition altered by lateral confinement? 16
5.2. Thermal contribution of the sidewall to the transition 17
6. Discussion: the Grenoble regime versus the Kraichnan regime **18**
7. Conclusion **20**
Acknowledgments **20**
Appendix. The Grenoble regime and the Boussinesq approximation **20**
References **24**

1. Introduction: an elusive regime

1.1. An historical perspective

In 1996, an abrupt enhancement of the heat transport efficiency (Nu) was reported in a convection cell driven at very high Rayleigh numbers (Ra) [1, 2] (the definitions of Ra and Nu are recalled later). This observation was understood as the signature of a new regime of convection, named the 'Ultimate Regime', and was interpreted following a prediction by R Kraichnan [3]. However, this observation was in apparent contradiction with some earlier $Nu(Ra)$ measurements, which did not evidence any new regime in nearly similar conditions [4]. This situation ignited a controversy that has grown over the years, as additional observations seemed to confirm both the transiting dataset from Grenoble and the non-transiting one from Chicago. Today, this issue is often considered as one of the most important open problems in convection and is driving experimental and numerical efforts worldwide. The ability to extrapolate laboratory results to environmental flows, for example, is strongly impaired by our lack of understanding of turbulent convection at very high Rayleigh numbers [5].

Table 1 summarizes the main specifications of Rayleigh–Bénard experiments reaching very high Ra. Bibliographic references are provided in the last column. For convenience, a name is attributed to each experiment performed in Grenoble (2nd column). Figure 1 presents measurements of the compensated heat transfer efficiency $Nu \cdot Ra^{-1/3}$ versus Ra. For completeness, a numerical simulation is included in the plot, while—for clarity—a few experiments from Grenoble are omitted. The Chicago data have been re-calculated using improved He properties fits and corrected for a sidewall spurious effect (see [6] for details

Table 1. Rayleigh–Bénard experiments reaching very high Ra.

Experiment		Marked transition[a]		Cell		Top/bottom plate		Sidewall		
Location	Name-Comment	$Ra \in 10^{11}$–10^{13}	Fluid	Height h (cm)	Aspect ratio Γ $\frac{\phi}{h}$ or $\frac{l}{h} : \frac{l}{h} : 1$	Thickness h_{plate} (cm)	Material	Thickness e (mm)	Material	References
Grenoble	*Chavanne*	•	He cryo	20	0.5	2.5/2.5	Cu/Cu	0.5	SS[b]	[2, 9, 10]
Grenoble	*Corrugated*	•	He cryo	20	0.5	2.5/2.5[c]	Cu/Cu[c]	0.5 − 0.6[c]	SS[b]	[11 12]
Grenoble	*Flange*	•	He cryo	20	0.5	2.5/2.5	Cu/Cu	0.5	SS[b]	The present work (see figure 2(d))
Grenoble	*Paper*	•	He cryo	20	0.5	2.5/2.5	Cu/Cu	0.16 + 0.5	Paper + SS[b]	The present work
Grenoble	*Cigar*	•	He cryo	43	0.23	2.5/2.5	Cu/Cu	0.5	SS[b]	[13] (see figure 11(b))
Grenoble	*Brass*	•	He cryo	20	0.5	2.5/2.5	Cu/brass	0.5	SS[b]	[12]
Grenoble	*Screen*	•	He cryo	20	0.5	2.5/2.5	Cu/Cu	0.5	SS[b]	The present work (see figure 10(b))
Grenoble	*Vintage*[d]	•	He cryo	20	0.5	2.5/2.5	Cu/Cu	0.5	SS[b]	The present work (see figure 9(b))
Grenoble	*CornerFlow*	•	He cryo	20	0.5	2.5/2.5	Cu/Cu	0.5[e]	SS[b]	[14]
Grenoble	*ThickWall*	•	He cryo	20	0.5	2.5/2.5	Cu/Cu	2.2	SS[b]	[14]
Grenoble	*Short*	•	He cryo	8.8	1.14	10/2.5	Cu/Cu	0.5	SS[b]	The present work (see figure 2(a)/(b)

Table 1. Continued.

Experiment		Marked		Cell		Top/bottom plate		Sidewall		
Location	Name-Comment	transition[a] $Ra \in 10^{11}$–10^{13}	Fluid	Height h (cm)	Aspect ratio Γ $\frac{\phi}{h}$ or $\frac{l}{h}:\frac{l}{h}:1$	Thickness h_{plate} (cm)	Material	Thickness e (mm)	Material	References
Chicago		–	He cryo	40	0.5	6/2	Cu/Cu	1.5	SS[b]	[4]
Rehovot	*Non-Boussinesq*[f]	–	SF6	10.5	0.73 : 0.73 : 1	1.9/?	Sapphire/Ni	Plexi/fluid/?		[15]
Oregon		–	He cryo	100	0.5	3.8/3.8	Cu/Cu	2.67	SS[b]	[16]
Trieste		•	He cryo	50	1	3.8/3.8	Cu/Cu	0.17[g] + 2.67	Mylar + SS[b]	[17]
Trieste	*Non-Boussinesq*[f]	?	He cryo	12.5	4	3.8/3.8	Cu/Cu	2.67	SS[b]	[18]
Göttingen 2009		–[h]	SF6	224	0.5	4/3.5+ 0.5 + 2.5	Cu/Cu-i-Cu[i]	Plexi/fluid/ shield		[19]
Delft	*TRANS simulation*	•	–[j]	–	8 : 8 : 1	–	–	–	–	[20]

[a] The bullet indicates that a steep enhancement of heat transfer is found above an Ra threshold within 10^{11}–10^{13} (with the $Nu(Ra)$ scaling exponent significantly larger than $1/3$).
[b] SS: stainless steel.
[c] The Cu plates had 0.11 mm deep grooves spaced by 0.44 mm. A corrugated bottom brass plate with 0.145 mm deep grooves spaced by 0.45 mm has also been used (see [12]). The sidewall was 0.6 mm thick with 0.1 mm deep grooves in it.
[d] The main difference between this cell and the *Chavanne* cell is a 1.3° or 3.6° tilt with respect to the vertical direction.
[e] An adjustable heating (cooling) ring is varnished on the external side of the sidewall, right above (below) the bottom (top) plate.
[f] The non-Boussinesqness of the data was acknowledged by the authors of these measurements.
[g] The Mylar sheet was epoxied. Two additional Mylar strips of height cover the 'flange region 2.5 cm (thickness 0.167 mm) just above the bottom plate and also below the top plate'.
[h] Recent unpublished data obtained with this cell evidence improved heat transfer near $Ra \simeq 4 \times 10^{13}$.
[i] The bottom plate consists of a Cu-epoxy-Plexiglass-epoxy-Cu sandwich. An aluminium composite plate has also been used.
[j] Boussinesq equations are simulated for $Pr = 0.71$

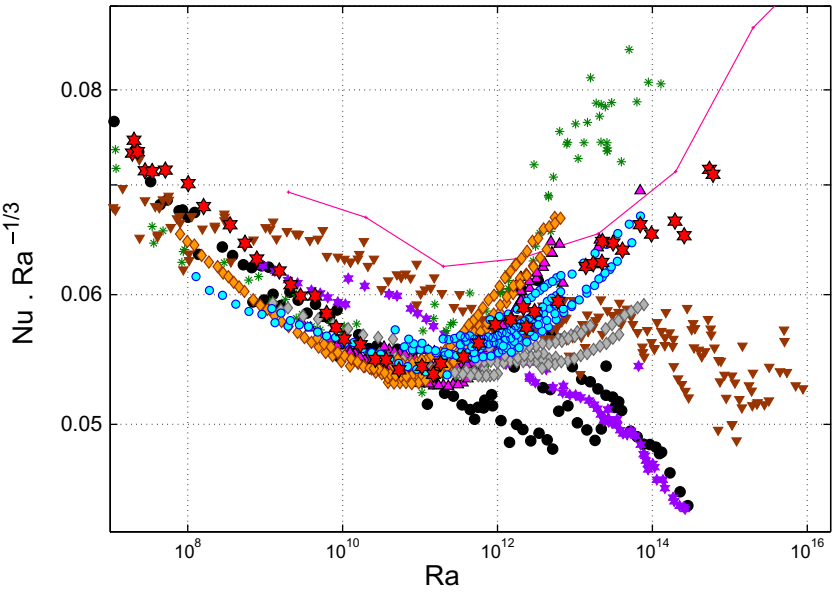

Figure 1. Compensated heat transfer $Nu \cdot Ra^{-1/3}$ versus Ra for very-high-Ra experiments in a cylindrical cell of aspect ratio $0.5 \leqslant \Gamma \leqslant 1.14$ and for $0.6 < Pr < 7$. Datasets from Grenoble (green asterisks (*Chavanne* cell, $\Gamma = 0.5$), magenta pointing-up triangles (*Vintage* cell, $\Gamma = 0.5$), blue discs (*Flange* cell, $\Gamma = 0.5$), grey diamonds (*Paper* cell, $\Gamma = 0.5$), orange diamonds (*Short* cell, $\Gamma = 1.14$), Trieste (red stars, $\Gamma = 1$), Oregon (brown pointing-down triangles, $\Gamma = 0.5$), Göttingen (purple stars, $\Gamma = 0.5$) and Chicago after correction (see text) (black discs, $\Gamma = 0.5$). The line corresponds to Delft T-RANS numerical simulations in an aspect ratio 8 : 8 : 1 cell.

of both corrections). This figure clearly illustrates that below $Ra \sim 10^{11}$, all experiments are in reasonable agreement, while different trends appear above $Ra \sim 10^{11}$. Indeed, the compensated heat transfer $Nu \cdot Ra^{-1/3}$ decreases with Ra in some experiments (Chicago, Oregon and Göttingen), while it increases in others (Grenoble and Trieste), leading to a nearly 100% difference in heat transfer efficiency around $Ra = 10^{14}$.

The convection community does not agree on the description of the results at very high Ra. For example, a recent review of convection concludes, '*Though the Grenoble experiments suggest such a transition near* $Ra = 10^{11}$ *neither the Oregon–Trieste experiments nor numerical simulations do so. The reason for the discrepancy is presently unresolved* [. . .].' [7], while we tend to consider that the Trieste experiment (red star in figure 1) and the Delft simulations (continuous line in figure 1) rather seem to fall under the group of transiting cells. Besides, we will argue in section 3 that the cited experiments are not in disagreement.

The terminology used in the literature probably adds to the confusion. For example, the adjective 'ultimate' introduced by Chavanne *et al* to name the new regime found in Grenoble has been used in the literature to refer to four different items: (i) the regime observed in Grenoble (regardless of its interpretation), (ii) the concept of asymptotic regime of convection, (iii) Kraichnan's model and (iv) a homogeneous turbulent flow forced by a thermal gradient [8]. To avoid any confusion, we will avoid referring to 'Ultimate Regime' or 'Ultimate State', and we will use the term 'Grenoble regime' for the regime that has been found and studied in Grenoble over the last 15 years.

The definitions of the Rayleigh, Prandtl and Nusselt numbers are

$$Ra = \frac{\alpha \Delta h^3 g}{\kappa \nu}, \quad Pr = \frac{\nu}{\kappa}, \quad Nu = \frac{P}{P_{\text{diff}}},$$

where α, κ, ν, g and h are, respectively, the isobaric thermal expansion coefficient, the molecular thermal diffusivity, the kinematic viscosity, the gravitational acceleration and the cell height. P_{diff} is the heat flux that would diffuse through the cell if the fluid was quiescent. The total heat flux P transported across the cell and the temperature difference Δ driving the flow are corrected to take the adiabatic gradient into account. We recall that this correction is exact.

1.2. Motivation and organization of the paper

The initial motivation for this paper was the two questions given below. They are addressed varying independently the Rayleigh number (within $10^8 < Ra < 6 \times 10^{14}$) and the Prandtl number (within $0.6 < Pr < 7$), in order to disentangle the influence of these two control parameters. Thus, we ask:

1. What is the nature of the Grenoble regime? In particular, is it the regime predicted by Kraichnan?
2. What are the triggering conditions of the Grenoble regime? As recalled later, Kraichnan's model does not describe the transition region, which leaves us with no precise prediction.

To address these questions, we performed a set of experiments that are described in section 2. The subsequent three sections explore the roles of the Prandtl number (section 3), the large-scale circulation (LSC) of the flow (section 4) and the sidewall of the cell (section 5) in the triggering of the Grenoble regime. Section 6 summarizes the characteristics of this regime and discusses them in connection with Kraichnan's model. Finally, the appendix presents a systematic study of non-Boussinesq effects, both experimental and theoretical.

2. New very-high-resolution cryogenic He experiments

The seven cryogenic convection cells of the present study are named the *Flange*, *Paper*, *Cigar*, *Screen*, *Vintage*, *ThickWall* and *Short* cells. All of them are cylindrical with diameter $\Phi = 10$ cm and height $h = 8.8$ cm (*Short* cell), 43 cm (*Cigar* cell) and 20 cm (all the others), corresponding to aspect ratios $\Gamma \simeq 1.14,\ 0.23$ and 0.50, respectively (see figures 2 and 3).

The various top and bottom plates are 2.5 cm thick, except for the conical top plate appearing in figures 2(a) and (b), which is 10 cm thick (*Short* cell). The conductivities of two Cu plates have been measured *in situ*, as described in [14], and we found 880 and 1090 $\text{Wm}^{-1}\,\text{K}^{-1}$ at 4.2 K for standard and OFHC Cu, respectively. The other plates, most of them made of annealed OFHC Cu, are expected to have thermal conductivities of the same order. The heat capacity of the bottom plates (sidewall flange and screws included) has been measured to be $\sim 1\,\text{J}\,\text{K}^{-1}$. The measured roughness of all these Cu plates is typically $ra \simeq 0.15 - 1\ \mu$m, depending on the cell, where ra is the arithmetic average of the absolute vertical deviation (often noted R_a). The flatness of the surfaces in contact with the fluid was typically within $\pm 4\ \mu$m for all cells except for one cell that had a 15 μm deep bump on one side. For the record, the non-corrugated brass plate used in a previous experiment [12] had a roughness of $ra \simeq 1\ \mu$m and a flatness within $\sim \pm 10\ \mu$m.

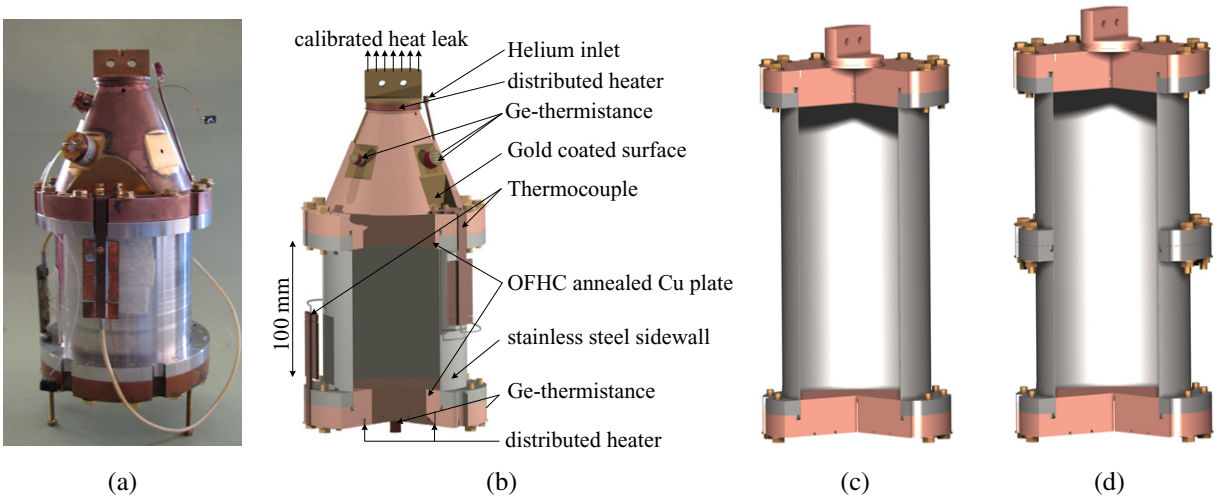

Figure 2. Cells before being hung in a cryogenic-vacuum chamber: (a) and (b) aspect ratio $\Gamma = 1.14$, *Short* cell; (c) aspect ratio $\Gamma = 0.50$, typical cell; (d) *Flange* cell.

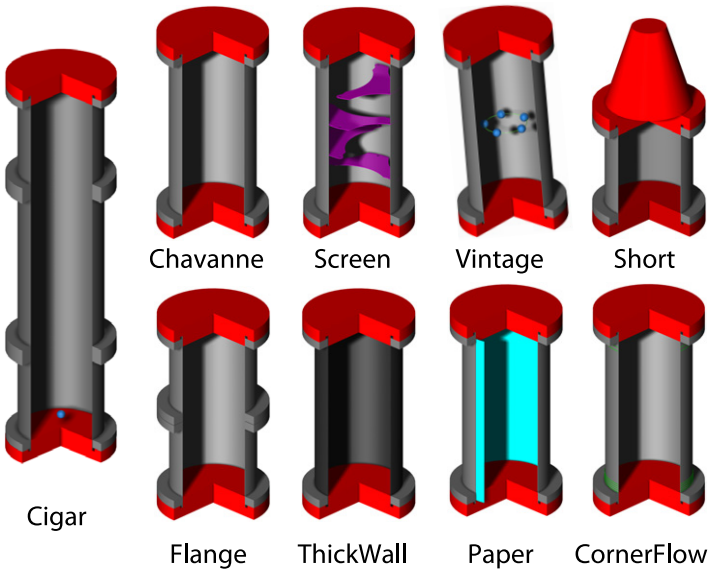

Figure 3. Schematics of the Grenoble cells discussed in this work.

Several seamless stainless steel sidewalls have been used that had a thickness of 2.2 mm (*ThickWall* cell) and $500 - 550\,\mu$m (all the other cells). The sidewall thermal conductance of each sidewall was measured *in situ*. The sidewall conductance of the *Paper*, *Screen* and *Vintage* cells was $327\,\mu\mathrm{W\,K^{-1}}$ at 4.7 K. The *Flange*, *Short*, *ThickWall* and *Cigar* cell sidewall conductances were, respectively, 1.15, 2.3, 4.8 and 0.5 times larger. The sidewall of the *Flange* cell was assembled using two sidewalls of aspect ratio close to unity (see figure 2(d)); the motivation was to mimic the design of the Oregon cell. The parasitic contribution of sidewalls on Nu was corrected using the analytical model from [21], confirmed in [22]. This correction is very small at the very high Ra of interest. For instance, around $Ra = 10^{12}$, the absolute value of the local scaling exponent of the heat transfer law, $Nu(Ra)$ would be typically 0.01 larger

without correction. The connection between the plate and the sidewall is detailed in [14]: it is such that the bottom (top) flange of the sidewall lies below (above) the bottom (top) plate-fluid interface to avoid parasitic contribution of the flange.

The cells hang vertically in a cryogenic-grade vacuum, except for the *Vintage* cell, which was tilted by 1.3° and 3.6°. The top plate is cooled by a helium bath at 4.2 K through a calibrated thermal resistance (typically $2\,\mathrm{K\,W^{-1}}$ at 6 K). The temperature is regulated by a PID controller. A constant and distributed Joule heating P is delivered on the bottom plate. The heat leak from the bottom plate to the surroundings has been measured *in situ* in a few experiments ($\simeq 200$ nW at 4.7 K) and it is three to four decades smaller than the lowest heating applied on the bottom plate to generate convection. This leak is mainly due to the radiative transfer to the environment at 4.2 K. This excellent thermal control is one of the advantages of our cryogenic environment over room temperature convection experiments, along with the excellent thermal properties of the Cu, which provide isothermal plates to the highest heat flux [23].

The temperature difference Δ between the plates is measured with an accuracy down to 0.1 mK, thanks to specifically designed thermocouples. For comparison, the smallest Δ in our experiments are about 10 mK. The temperature of each plate is measured with various *Ge* thermistances. Their calibration is checked *in situ* against the critical temperature T_c of the fluid with a resolution of 0.2 mK. To avoid a common misunderstanding, we stress that all the $Nu(Ra)$ measurements are done far away from the critical point, as argued in the appendix. The critical point is simply used here as a thermodynamical reference to cross-check temperature calibration.

Cells are filled with various ^{4}He densities, ranging from dilute gas to liquid, and then closed with a cryogenic needle valve located close to the cell. The amount of He introduced into the cell is measured in a calibrated tank at room temperature, and it is occasionally cross-checked at low temperature by measuring the condensation temperature. A thermosiphon hanging in vacuum between the cryogenic valve and the cell prevents convective transfer in the filling line. He properties are calculated as described in [6]. Most of the measurements are performed for the temperatures and densities where the accuracy of He properties is the best; for example, at $T = 6\,\mathrm{K}$ or at about $\rho = 70\,\mathrm{kg\,m^{-3}}$ [6].

Figure 4 represents the *Vintage*, *Flange*, *Paper*, *Short*, *ThickWall*, *Screen* and *Cigar* cell datasets in the Ra–Pr parameter space. Contrary to a common misconception of cryogenic convection experiments, Ra can be varied at a given Pr, as illustrated in this figure and already in previous work (e.g. [4, 24]). Each subset of constant Pr data is obtained while working at a fixed mean temperature T and mean volumetric mass ρ. For each of these subsets, the local scaling exponent of the $Nu(Ra)$ law—that is, $\partial \log Nu / \partial \log Ra$—can be determined with high accuracy because the uncertainty of the fluid properties prefactors appearing in Nu and Ra vanishes. The local exponents determined for each of these experiments are plotted in figure 5. In such a plot, the transition to the Grenoble regime can be easily spotted by the increase in the exponent above the 1/3 value. We underline the variability of the transition, both in terms of transitional Ra (nearly two decades) and in terms of stiffness (exponent from 0.36 to 0.44 at $Ra \simeq 10^{14}$).

3. The Grenoble regime and the Prandtl number

This section compiles existing measurements and reports new ones on the interplay between the Prandtl number Pr and the Grenoble regime.

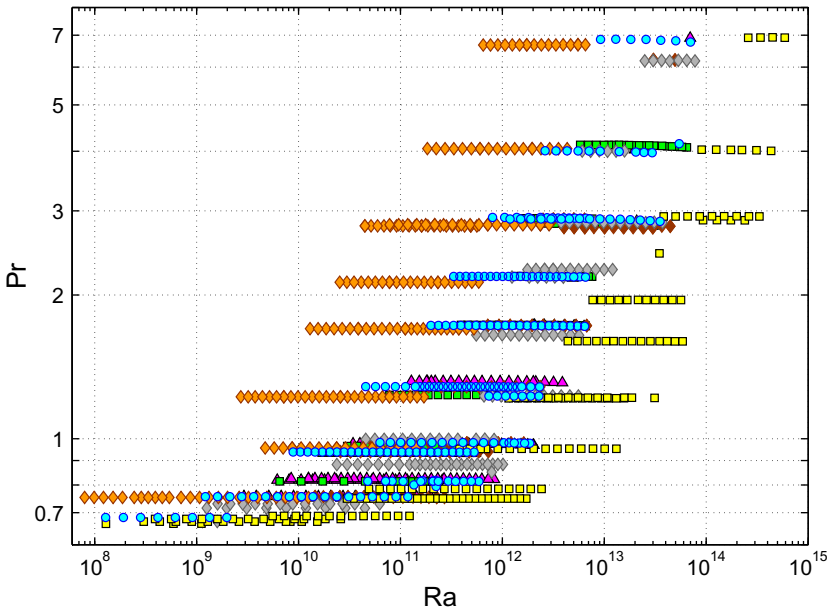

Figure 4. Parameter space for the datasets *Short* (orange diamonds), *Vintage* (magenta pointing-up triangles), *Flange* (blue discs), *Paper* (grey diamonds), *ThickWall* (green squares), *Screen* (brown diamonds) and *Cigar* (yellow squares) cells.

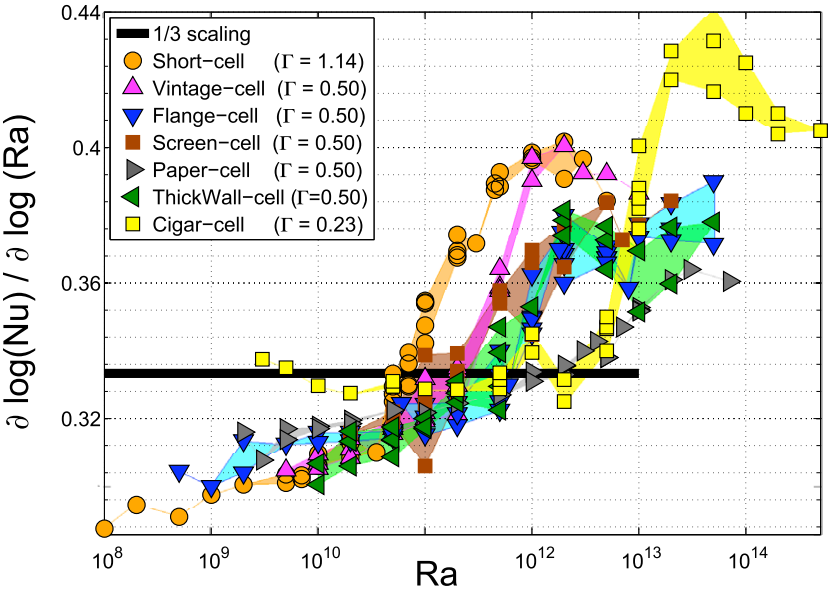

Figure 5. Local exponent of the $Nu(Ra)$ law in various Rayleigh–Bénard cells for $0.6 < Pr < 7$.

3.1. Grenoble regime in the Ra–Pr parameter space

Figure 6(a) gathers various very-high-Ra measurements in cylindrical aspect ratio $\Gamma = 0.5$ Rayleigh–Bénard cells. The yellow area encircles all the measurements taken in the Grenoble

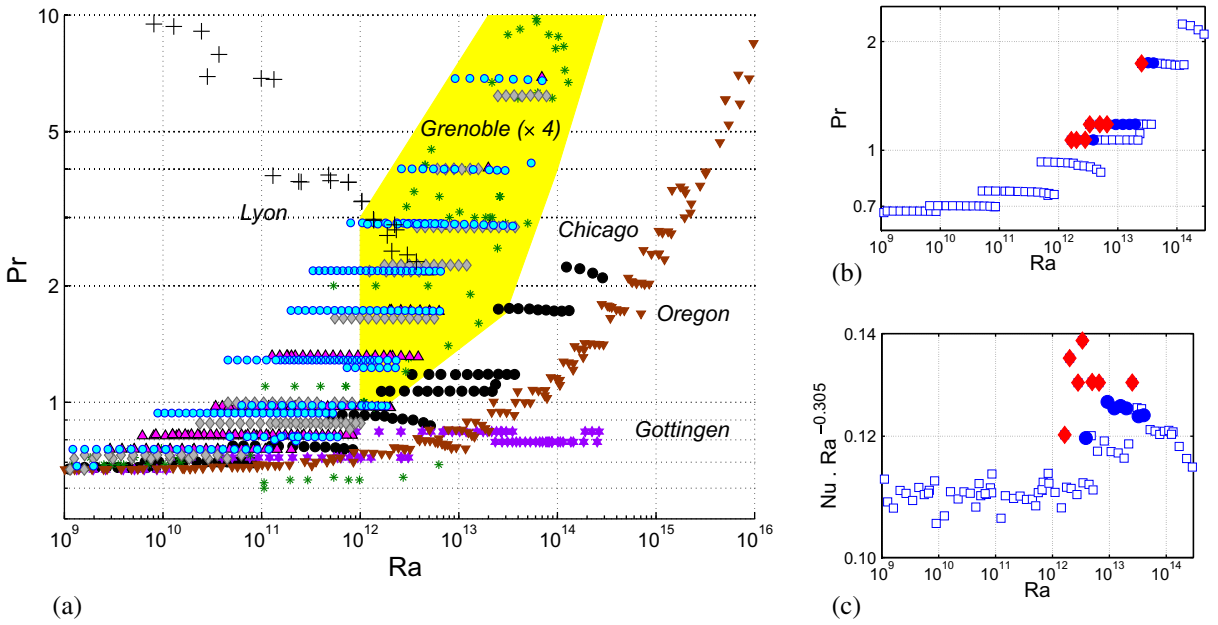

Figure 6. Left: parameter space of very-high-Ra experiments with aspect ratio $\Gamma = 0.5$. Right: Chicago dataset. The points that are closest to the yellow area are marked with full symbols (blue discs and red diamonds for the closest ones), while the others are plotted with open squares.

regime. Conversely, nearly all the datasets reaching very high Ra without experiencing a (clear) transition fall outside this area. A few points from Chicago fall close to this area. Very interestingly, these points seem to experience a small heat transfer enhancement, as shown in figure 6 (right-side subplots). Another interesting point is the Chavanne *et al* points for $0.6 < Pr < 0.7$ and $10^{11} < Ra < 10^{13}$: no heat transfer enhancement is distinguishable on these points, which is consistent with the location in the Ra–Pr parameter space. As a first point, it is worth stressing that the cryogenic data from Grenoble, Chicago and Oregon are not in disagreement as long as differences in Pr are regarded. As a second point, in addition to the very high Ra condition, the transition is favoured above a $Pr(Ra)$ threshold. The only possible contradiction between these very-high-Ra datasets may be found at about $Pr \sim 2$–3, with the Lyon water experiment [25], which reported no transition. The corresponding dataset seems to be in contradiction over half a decade of Ra, right above the transition. We will show that the transition threshold can greatly vary from one cell to another depending on the sidewall boundary conditions (section 5). This may explain the apparent contradiction. Another possible explanation is accuracy issues at the highest Ra in room temperature experiments due to significant correction of plate effects, which could mask the onset of a transition. Further investigations in this region of the parameter space, with smaller He cells and larger water cells, would be useful.

Unfortunately, due to lack of available experiments, it is not yet possible to generalize this Ra–Pr phase-space description to cells with other aspect ratios and shapes. However, we will show in section 5 that the transition Ra has a strong aspect-ratio dependence in the range $0.23 \leqslant \Gamma \leqslant 1.14$, at least for Pr of the order of one.

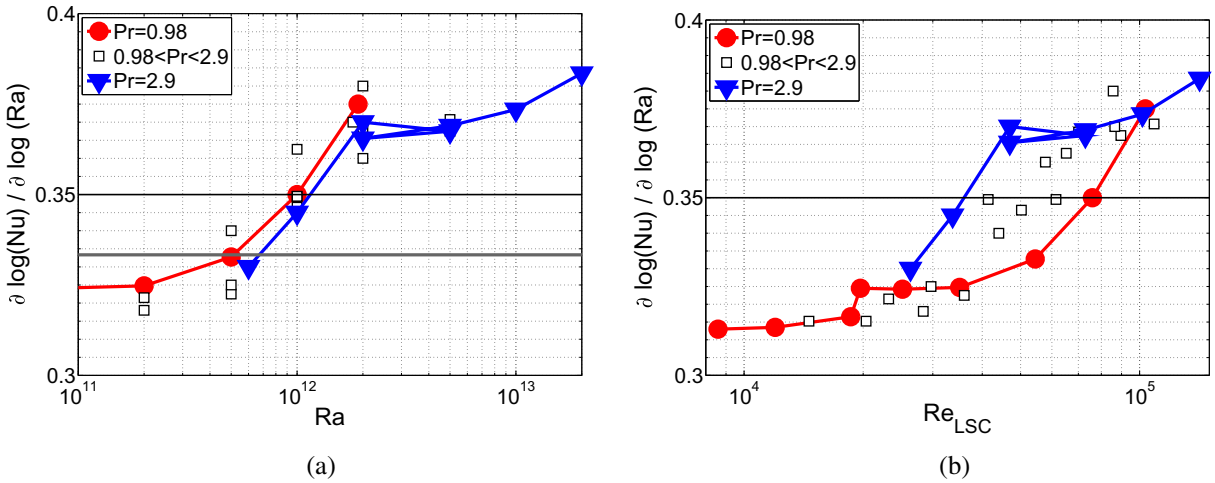

Figure 7. Local exponent of the $Nu(Ra)$ dependence for various Pr in the *Flange* cell ($\Gamma = 0.50$): (a) versus Ra and (b) versus the Reynolds number of the LSC.

3.2. Prandlt number dependence of the Grenoble regime

Does the Ra of the onset of the transition depend on Pr? Figure 7(a) gives the local scaling exponent of $Nu(Ra)$ around the transition within $0.98 \leqslant Pr \leqslant 2.9$. As can been seen, there is no Pr dependence of the transition Ra, within accuracy, in this limited range of Pr.

As we will show later, the Reynolds numbers associated with the LSC in our $\Gamma = 0.5$ cells roughly scale like $Re_{\mathrm{LSC}} \simeq 0.13 Ra^{0.5} Pr^{-0.75}$ (see figure 8(b)). If the transition was triggered when Re_{LSC} reaches a critical value, a threefold increase in Pr would shift the transitional Ra by a factor of $3^{0.75/0.48} \simeq 5.6$. This is not compatible with the result presented in figure 7(a), which indicates a weaker—if any—dependence. Figure 7(b) presents the same exponents versus Re_{LSC} (estimated with the above fit) and shows that the transition does not occur for a unique value of Re_{LSC}. A similar conclusion can be drawn for the aspect ratio $\Gamma = 1.14$ cell over the same range of Pr. This suggests that the transition is not simply triggered by the LSC shear on the boundary layers. We will confirm this important result later.

Figure 8(a) shows the $Nu(Ra)$ local scaling exponent versus Pr over a limited window of very high Ra, and for three cells with aspect ratio from 0.23 to 1.14. The Ra-window is chosen significantly above the transitional Ra of each cell, with the purpose of being in the region where the new regime is well established. No systematic dependence of the local exponent versus Pr is detectable within uncertainty for $1.2 \leqslant Pr \leqslant 6.8$. The best fit for $Nu(Pr)$ at constant and high Ra gives $Nu \sim Pr^{0.045}$.

As a conclusion to this section, a first requirement for the occurrence of a transition is that the Rayleigh number is above a Pr-independent threshold. In aspect ratio $\Gamma = 0.5$ cells, a second requirement has been evidenced: Pr should be above an Ra-dependent threshold. Both requirements are summarized by the phase space of figure 6. Once the transition has occurred, the Prandtl number is found to have a small—if any—effect on heat transfer. We recall that our analysis focuses on the range $1 \lesssim Pr \lesssim 7$. It is therefore possible that this window of Prandtl numbers sits near the frontier between a low-Prandtl-number regime and a high-Prandtl-number regime.

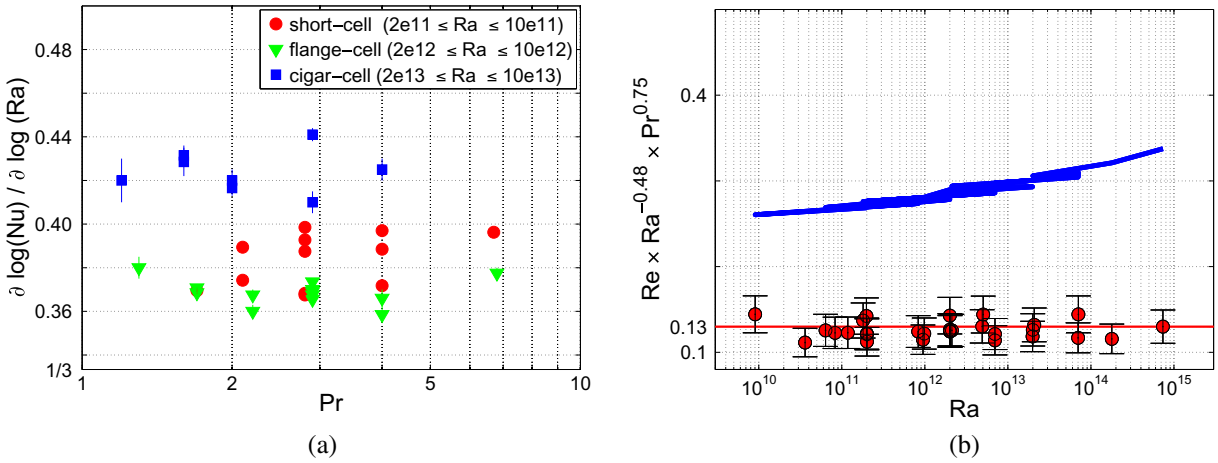

Figure 8. (a) Local exponent of the $Nu(Ra)$ dependence versus Pr for the highest Ra in cells of aspect ratios $\Gamma = 1.14$, 0.50 and 0.23. (b) Compensated Re associated with the LSC for $\Gamma = 0.50$. Red discs: based on measurements of Re_{LSC}. Blue segments: Re based on a local velocity fit at mid-height (and at a distance $\Phi/4$ from the cell axis) measured previously in the same cell [9].

4. The Grenoble regime and the Large-Scale Circulation (LSC)

A LSC is often present in turbulent RB convection [26]. This 'wind' has complex dynamics with multistability, reversals and quiet periods. One of the oldest hypotheses to explain the puzzle at very high Ra was to invoke an interplay with the LSC ([27], p 70). We report below a few tests of the interplay between the wind and the Grenoble regime.

4.1. Is the wind changing when the transition occurs?

The correlation between the LSC and the Grenoble regime can be assessed by comparing the statistics of the LSC below and above the transition. To probe the LSC, five thermometers [28] are suspended within the flow, in the horizontal mid-plane of the *Vintage* cell. They are evenly distributed around the circle that is equidistant from the cell axis and the sidewall (see figure 9(b)). Temperature time series are recorded simultaneously from the five thermometers. The Reynolds number associated with the LSC was determined using the auto-correlation technique. A LSC turnover timescale T_{LSC} is defined imposing that the auto-correlation of one of the thermometers (the most sensitive one was used) has its first minimum at $T_{\mathrm{LSC}}/2$. Physically, this characteristic timescale can be understood as the time-of-flight of the large-scale temperature heterogeneities from one side of the cell to the other side. The Re associated with this LSC time is then defined as

$$Re_{\mathrm{LSC}} = \frac{2h^2}{\nu \cdot T_{\mathrm{LSC}}}.$$

Figure 8(b) shows Re_{LSC} over five decades of Ra and within $0.76 \leqslant Pr \leqslant 6.88$. We stress that Ra and Pr are varied independently, as can be seen in figure 4, which enables us to

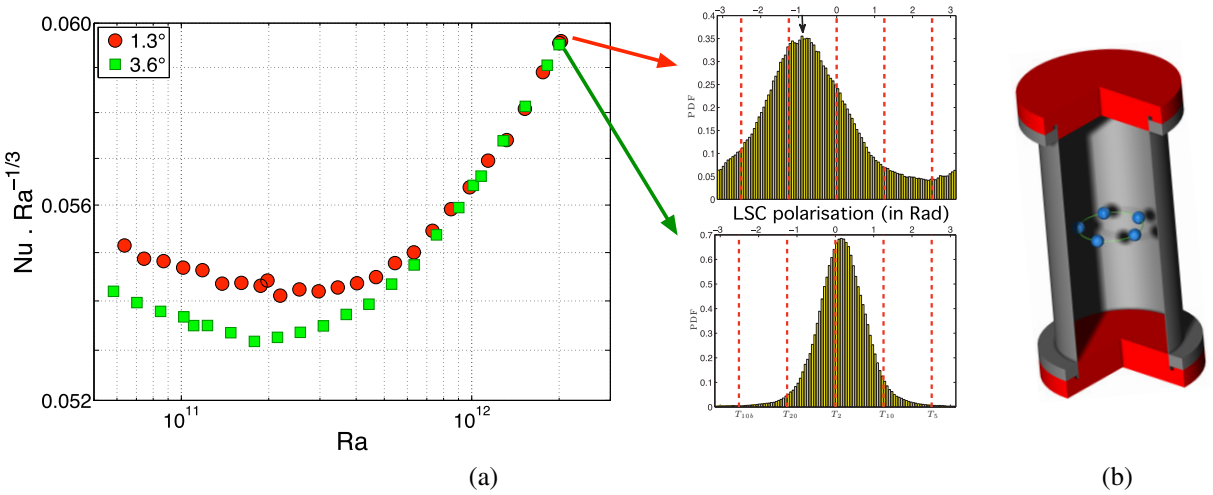

Figure 9. (a) Heat transfer (left figure) and probability density functions (pdfs) of the LSC angular direction at $Ra = 2 \times 10^{12}$ in the same cell with a 1.3° tilt (discs and upper pdf) and with a 3.60° tilt in a different direction (squares and lower pdf) for $Pr = 1.0$. (b) Schematic diagram showing the probe positions in the *Vintage* cell. The probe sizes and the tilt are exaggerated for visibility.

disentangle their relative contribution and fit the exponents of both Ra and Pr independently. The compensation chosen on the y-axis illustrates the best power-law fit,

$$Re_{\mathrm{LSC}} \simeq (0.13 \pm 0.03) \times Ra^{0.48\pm0.02} \times Pr^{-0.75\pm0.03}.$$

This fit is in agreement with other ones that have been reported in the literature at lower Ra, in the hard turbulence regime (e.g. [29]–[31]). The important result here is that this fit also remains valid in the Grenoble regime. In particular, no discontinuity is detectable at the transition.

The Reynolds number Re_{local} based on a previous local velocity measurement at mid-height in a similar cell is also plotted in figure 8 [9]. The difference in magnitude and scaling between Re_{LSC} and Re_{local} is consistent with the differences in their definition (e.g. [30])[2]. This previous determination of an LSC Reynolds number, as well as a third one carried out in the Trieste (transiting) cell [33], also confirms that the strength of the LSC has no discontinuity when the transition occurs.

To complete the characterization of the LSC, the statistics of its angular direction or 'polarization' are measured. At each time step of the temperature time series, the temperature distribution along the rack of five probes is Fourier transformed versus angular position. The strength and polarization of the LSC versus time is defined from the amplitude and phase of the first Fourier mode. Similar multi-probe techniques have been validated to analyse the LSC in previous studies (e.g. [34, 35]). When the amplitude of the first mode is smaller than

[2] The local velocity measurement was performed using two thermometers, one above the other, and by inferring the velocity from the cross-correlation of the two-temperature time series [9]. The slight difference in scaling ($Re_{\mathrm{LSC}} \sim Ra^{0.48}$ versus $Re_{\mathrm{local}} \sim Ra^{0.49}$) can be understood easily: the turnover time scale T_{LSC} is seen as the ratio of an effective LSC path length to its effective velocity. If we imagine that the effective path length of the LSC slightly evolves with Ra, we immediately find that Re_{LSC} and Re_{local} should have slightly different scalings [32].

1.3 times the rms amplitude of higher modes, we consider the LSC as indistinguishable from the background fluctuations. In this case, the LSC is considered to be undefined. Systematic measurements of the probability density functions (pdfs) of the LSC polarization are done from $Ra = 3.6 \times 10^{10}$ to $Ra = 2 \times 10^{12}$ (and $Pr \simeq 1$). Examples of such pdfs are displayed in figure 9(a). No significant discontinuity of these pdfs is detectable at the transition, in particular on the shapes and maximum value of the pdfs. Similarly, the fraction of time during which the LSC is considered as undefined remains constant ($29\% \pm 5\%$) over the whole range of Ra.

As a first conclusion about the wind, we showed that the occurrence of the transition is not associated with a discontinuity in strength, scaling or polarization of the LSC. One consequence is that the transition is not triggered by some instability in the dynamics of the LSC. Another consequence is that the transition does not alter the LSC significantly.

4.2. Is the transition altered by modifications of the LSC?

The conclusion above does not rule out the possibility that the transition to the Grenoble regime is triggered by the LSC, in particular by its strengthening with Ra. To explore how the transition depends on the LSC, we first altered it by introducing some external constraints on the flow.

A first test consists in tilting the *Vintage* cell from 1.3° to $3.60 \pm 0.15^\circ$ in a different direction. The set of thermometers inside the flow (see the previous subsection) confirms that the LSC polarization follows the new tilt direction and that its angular distribution becomes sharper when the tilt angle is larger, as shown by the pdfs of figure 9(a). Below the transition, increasing tilt reduces heat transfer by 2%, consistent with other experiments with the same aspect ratio [36, 37]. In contrast, the heat transfer is unchanged in the Grenoble regime. This robustness of the heat transfer to a tilt increase (and to a more pronounced polarization of the LSC) is a new signature of the Grenoble regime.

Is the transition triggered by the shearing of the boundary layers by the LSC? In section 3.2, we reported some indirect evidence that this was not the case. We performed here a more direct test of this mechanism by breaking the LSC with screens to see if the transition was disfavoured. Similar tests have been performed in the past to explore the role of the LSC in the hard turbulence regime [38, 39]. Four croissant-shaped thin horizontal plastic screens are evenly distributed along the height of the *Screen* cell (see figures 10(b) and (c)). The angular distribution of screens is helicoidal, with a 90° angle between consecutive ones. The surface of each screen equals 33.3% of the cell cross-section. Figure 10(a) presents heat transfer measurements in this cell and in a similar cell without screens but with a residual tilt of 1.3° to break the axisymmetry (*Vintage* cell). The measurements have been performed for five sets of mean temperature and mean density conditions. This allows a one-by-one comparison of both experiments independently of the fluid properties.

Within accuracy, the transition occurs for the same threshold Ra as can be seen for the dataset at $Pr \simeq 0.75$ and $Pr \simeq 0.98$. This suggests that the transition to the Grenoble regime in aspect ratio $\Gamma = 0.50$ cells is not triggered by the LSC. This is the main result of this specific experimental study. Additionally, over two decades of Ra above the transition, the heat transfer of both experiments is within 6%. Thus, a strong alteration of the LSC has a limited effect on heat transfer efficiency in the Grenoble regime in this range of Ra and Pr.

Finally, a third indication of the limited influence of the LSC on the transition threshold is provided by the $\Gamma = 0.23$ *Cigar* cell. As shown in figure 11, the heat transfer is multi-valued around $Ra \simeq 10^{12}$–10^{13} with $\sim 14\,\%$ difference in Nu for a given Ra. In such an elongated

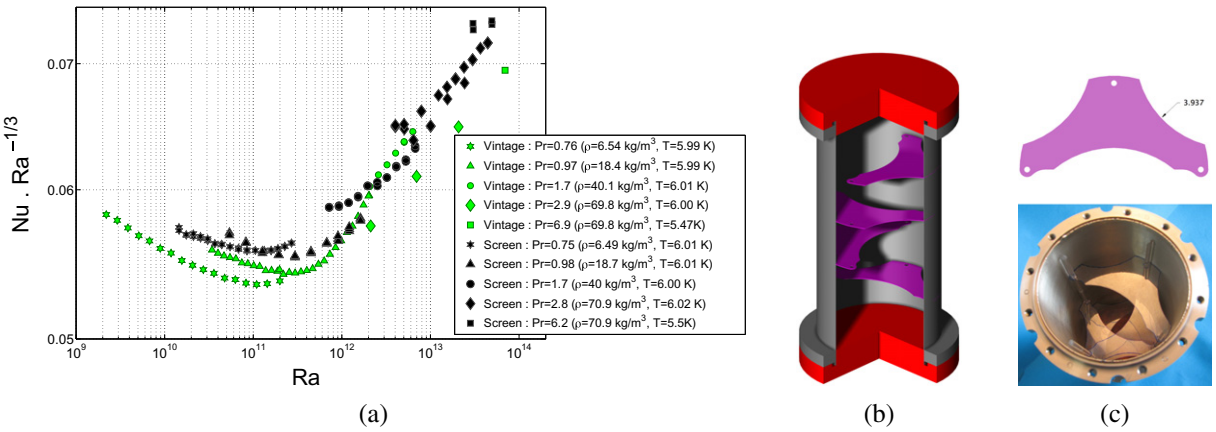

Figure 10. (a) Heat transfer in a cell with four screens breaking the LSC (black symbols, *Screen* cell) and in a reference cell without screens (green symbols, *Vintage* cell). (b) Schematic diagram showing the screen position in the *Screen* cell. (c) Photograph of the cell interior and schematic diagram of one screen.

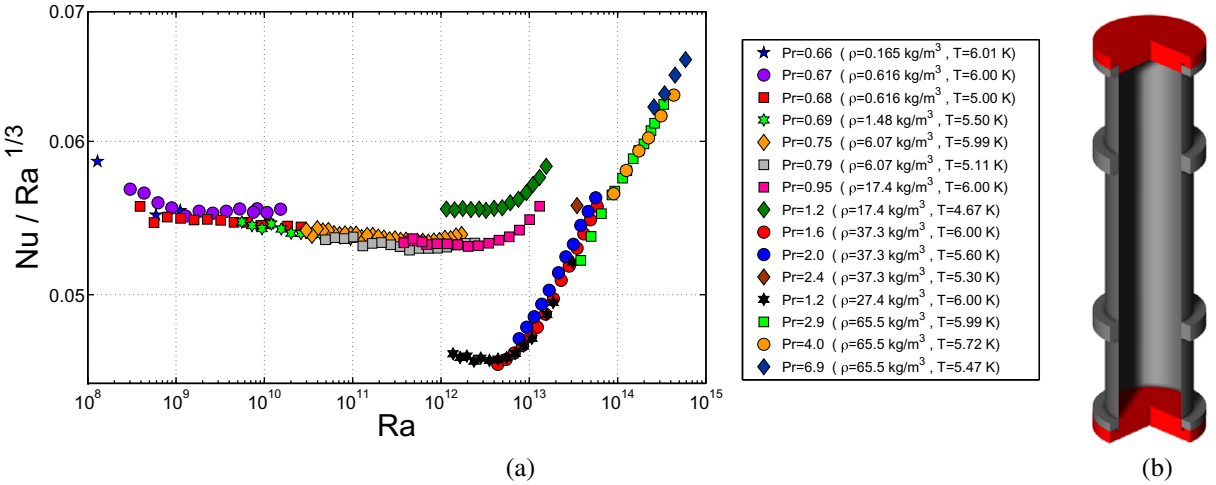

Figure 11. *Cigar* cell ($\Gamma = 0.23$). (a) Compensated heat transfer. The chronological order of the data acquisition is given by the legend, from top to bottom. (b) Schematic diagram of the cell.

cell, the LSC can be organized in one or several rolls on top of each other. We interpret the bi-valued Nu as a signature of transition from one LSC configuration to another one. A similar effect has been reported in the past with a small percentage difference in Nu in a $\Gamma = 0.5$ cell, which was interpreted as the first evidence of the multistability of the LSC in turbulent convection [24][3]. The transition to the Grenoble regime happens to occur in the window where

[3] Interestingly, although the LSC multistability has been confirmed by simulations [40] and adopted by the community, the original heat transfer measurements have been questioned by some groups failing to reproduce them with water. This may illustrate one of the advantages of a cryogenic environment for precise heat transfer measurements: the plates have a very low thermal inertia and a very high diffusivity (compared to He), so they do not alter the LSC dynamics.

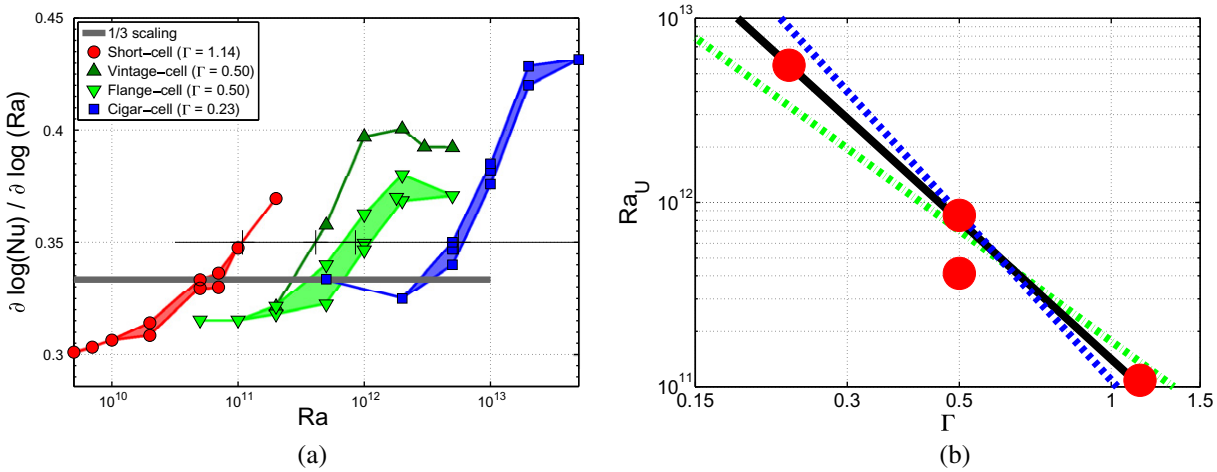

Figure 12. Aspect-ratio dependence of the transitional Ra. (a) Local scaling exponent of $Nu(Ra)$ for $Pr = 1.5 \pm 20\%$ in cells with rather similar sidewalls, but aspect ratio from $\Gamma = 0.23$ to $\Gamma = 1.14$. (b) Ra_{U} versus aspect ratio. The lines correspond to $Ra_{\mathrm{U}} \sim \Gamma^{-2}$, $\Gamma^{-2.5}$ and Γ^{-3}.

Nu is multi-valued, giving the opportunity to compare the transition for both configurations of the LSC. Within resolution, the transition occurs for the same Ra and is as steep for the two mean flows.

To conclude this section, we first recall that the heat transfer in the hard turbulence regime is hardly altered by changes in the LSC. In particular, it is well known that a cell tilting or the presence of screens inside the cell mostly results in a change in the prefactor of the $Nu(Ra)$ scaling. In this section, we found that these properties are also satisfied in the Grenoble regime. A second and more surprising conclusion is that the transition to the Grenoble regime is not directly triggered by LSC for Pr of the order of unity, contrary to what has often been assumed in the literature since 2001 when discussing the transition mechanism (e.g. [7, 9, 17, 41]).

5. The Grenoble regime and sidewall

5.1. Is the transition altered by lateral confinement?

Figure 12(a) presents the local scaling exponent of $Nu(Ra)$ in cells with aspect ratios $\Gamma = 1.14$ (*Short* cell), $\Gamma = 0.50$ (*Vintage* and *Flange* cells) and $\Gamma = 0.23$ *Cigar* cell. All these cells have the same diameter Φ, their sidewalls are made of the same material ($\sim$0.5 mm-thick stainless steel) and the fluid Prandtl number is the same ($Pr = 1.5$) within $\pm 20\%$. An arbitrary threshold exponent of 0.35 is used to define a transition Rayleigh number Ra_{U} for each cell and this quantity is plotted versus Γ in figure 12(b). We find a strong $Ra_{\mathrm{U}}(\Gamma)$ dependence, which is fittable as $Ra_{\mathrm{U}} \sim \Gamma^{-2.5}$ (solid line) but also remains compatible with a Γ^{-3} dependence (blue dashed line). The $Ra_{\mathrm{U}} \sim \Gamma^{-3}$ scaling can be interpreted stating that the transition occurs when a flow length scale that is proportional to the cell height h reaches a constant scale found in the four cells. What is this fixed length scale?

A first hypothesis is that this fixed scale is set by defects in the plates' surface. Systematic roughness and flatness/wavyness characterizations have been performed on all the plates ever

operated in Grenoble. We found that the characteristic scales of these defects (see section 2) are much smaller than the thermal boundary layer thickness $h/2Nu \sim 200\,\mu$m at the transition. Moreover, among cells with the same height, we did not find any correlation between the transition Ra and the plates' residual roughness, although some were 5 times rougher than others. Finally, we note that the Oregon and Trieste cells are made with the same plates: if a plate defect was causing the transition, the Oregon cell should have transited. Rejecting this first hypothesis, we retain the most obvious common length scale shared by the four cells: the cells' diameter Φ. The $Ra_U \sim \Gamma^{-3}$ scaling can then be reformulated stating that the transition occurs when the Rayleigh number based on Φ (instead of h) reaches a critical value, at least as a first approximation and within the limited range of aspect ratios $0.23 \leqslant \Gamma \leqslant 1.14$. Surely, these properties associated with the lateral confinement are not expected to extrapolate to an aspect ratio much larger than unity.

5.2. Thermal contribution of the sidewall to the transition

We found that confinement by sidewalls disfavours the transition. Is this confinement effect purely geometrical (presence of fixed lateral boundaries) or is it also coupled to the thermal properties of the sidewall? To explore this possibility, the thermal properties of the sidewall have been altered in three ways:

(i) *Paper* cell: three layers of smooth paper have been rolled against a 0.5 mm-thick stainless steel sidewall. This results in an increase in the sidewall roughness, a 165 μm-thick thermal insulation between the flow and the stainless steel sidewall, and an extra thermal inertia attached to the sidewall (the inertia of the He trapped in the paper is a few tens of times larger than the inertia of the stainless steel).

(ii) *ThickWall* cell: the sidewall has been made roughly 4.4 times thicker to increase the sidewall spurious thermal effects.

(iii) *CornerFlow* cell: a tunable heating (respectively cooling) ring has been installed on the outer side of the sidewall, near the bottom plate (respectively top plate) connection. This enables us to force more or less the corner flows expected at the plate–sidewall angle. An isolated heater was also varnished on the external side of the sidewall, 5 cm above the bottom plate. This heater enables us to break the axisymmetry of the sidewall.

Experiments (ii) and (iii) have been described in a conference proceeding [14]. It was found that these alterations of the sidewall have a very limited impact on the transitional Ra and on the strength of the transition (the $Nu(Ra)$ data of the *ThickWall* cell appear in figure 5). The *Paper* cell experiment is more surprising. As illustrated in figure 5, the local exponent of $Nu(Ra)$ increases more slowly with Ra than for the other cells, and the transition seems to occur at slightly higher Ra. We don't understand why the paper layers have such a strong effect on the steepness of the transition, but these results suggest that a thermal interaction between the sidewall and the flow can significantly alter the transition.

As a conclusion to this section, the transition seems significantly disfavoured by the lateral confinement of the sidewall. A practical consequence is that the transition is not easier to observe in elongated cells, because it occurs at higher Ra. We found that the transitional Ra and the transition sharpness can significantly vary from one cell to another depending on the sidewall properties. This observation raises issues regarding the modelling of the sidewall in very-high-Ra simulations.

6. Discussion: the Grenoble regime versus the Kraichnan regime

Over the last 14 years, the Grenoble regime has been characterized in various ways. We summarize the main observed features and discuss them in connection with Kraichnan's prediction.

(i) **The $Nu(Ra)$ scaling**. Kraichnan predicted the following heat transfer law,

$$Nu \sim \frac{Ra^{1/2}}{(\log Re)^{3/2}}. \tag{1}$$

We omit a Pr-dependent prefactor of the numerator, because the Pr dependence of the denominator is not considered in the model. A precise quantitative comparison of (1) with the measurements is difficult to justify, because this equation is only valid for asymptotic large Ra (*a priori*), as Kraichnan insists[4]. Nevertheless, this equation sets bounds on the local scaling exponent of $Nu(Ra)$ in the region joining the two regimes. Indeed, we expected this exponent to be larger than $1/3$ (hard turbulence regime) and lower than 0.5 (asymptotic exponent of (1)). This window of exponents is consistent with the exponents observed in the Grenoble regime (see figure 5).

A more quantitative test of the $Nu(Ra)$ scaling is nevertheless possible. Indeed, in the framework of the Kraichnan model, the boundary layer theory predicts that the denominator in (1) should be replaced by a constant if the plates are rough enough or corrugated. This test was performed (*Corrugated* cell) and a pure $Nu \sim Ra^{0.5}$ scaling was observed [11].

(ii) **Evidence of a boundary layer instability**. Analysing the shot noise generated by thermal plumes in the bottom plate, it was found that the Grenoble transition is indeed associated with an instability localized in the boundary layer [10]. This result is consistent with the occurrence of Kraichnan's regime, which is characterized by a laminar-to-turbulent transition of the velocity boundary layers lying over the heating and cooling plates.

(iii) **Transition on the fluid's temperature fluctuations**. Non-invasive measurements within the boundary layers are very delicate due to its small thickness. A direct test of the turbulent state of the boundary layer is therefore difficult. Nevertheless, it was found that the temperature fluctuations right above the bottom boundary layer do experience a change in statistics when transition occurs [42] (see also [9]).

(iv) **Weak influence of LSC**. In section 5, we found that breaking the LSC with screens has a limited impact on the heat transfer, although the LSC must have been significantly altered. Similarly, the transitions to the Grenoble regime had similar characteristics when occurring on two different configurations of the LSC in the *Cigar* cell. An increased tilt of the convection cell resulted in better clamping of the LSC polarization but did not result in lower Nu, as found in the hard turbulence regime. Finally, in section 3, we found that the transition did not occur for a fixed value of the LSC Reynolds number, at least for $0.98 \leqslant Pr \leqslant 2.9$.

The addition of all these observations clearly indicates that the LSC alone is not a transition trigger, as is often assumed in the literature. Once the transition has occurred, we

[4] 'In view of the inaccuracies inherent in the mixing-length approach, we think that it would be largely illusory to correct discrepancies of this kind by a more careful treatment of the joins between the various asymptotic regions' (from [3], p 1386).

find that the heat transfer is robust to alterations to the LSC, such modifications resulting mostly in new prefactors (of the order of 1) for the $Nu(Ra)$ law.

(v) **The transition Ra**. The transition Ra is found to be typically between 10^{11} and 10^{13}. Cell diameter and sidewall material given, the transition Ra was found to scale as $h^{2.5}$ for aspect ratios within 0.23–1.14. Thus, in this range, the transition Rayleigh number based on the cell diameter (instead of h) is nearly constant. These properties of confined cells are not expected to hold for aspect ratios much larger than unity.

In Kraichnan's model, the transition occurs when the eddies located in the bulk of the flow shear the velocity boundary layers beyond their stability point. As argued in [9], a transition at $Ra \simeq 10^{11}$ would be compatible with a boundary layer instability that would originate from the shearing by the LSC. Following this idea, various estimates based on different hypotheses suggest that any transition occurring in the window $Ra \simeq 10^{11}$–10^{15} (for $Pr \sim 1$) would also be compatible with Kraichnan's model (see e.g. [17, 41]). Unfortunately, we found that the transition cannot simply be triggered by the LSC. These estimations for the transition Ra should therefore be considered with much reservation. Alternatively, we could speculate that the destabilizing shearing of the boundary layer is caused by the velocity fluctuations above the boundary layers. This scenario is not incompatible with the results in section 4. The small Pr dependence of the transition near $Pr \simeq 2$ (section 3.2) could result from the proximity to the low Pr region. Thus, strictly speaking, the present results are not ruling out Kraichnan's model, but they are not supporting it either.

As a final remark possibly related to the Grenoble regime, the thermal and velocity boundary layers have been characterized at intermediate Ra (where they are thick enough to be resolved) in room temperature experiments. Extrapolation of their properties over three decades of Ra suggests the occurrence of a transition compatible with Kraichnan's views near $Ra \simeq 10^{13}$ [43, 44].

(vi) **Transition in the Ra–Pr parameter space**. In section 3, we showed that all $\Gamma = 0.5$ experiments reporting a transition are localized in the same region of the Ra–Pr parameters space and that nearly all the experiments without transition fall outside this region. There is no understanding of this parameter space. Updating Kraichnan's model using the knowledge gained over the last 50 years would certainly be highly interesting.

(vii) **A threshold exponent 1/3?** For most Grenoble cells, the transition seems to occur abruptly when the local exponent of $Nu(Ra)$ reaches the value 1/3, as illustrated in figure 5. Conversely, the exponent 1/3 is not reached in most of the very-high-Ra experiments that do not report a transition, as illustrated in figure 1. Interestingly, the exponent 1/3 is found in the Malkus model of uncoupled boundary layers [45]. We have no interpretation for these coincidences.

(viii) **Thermal interaction with the sidewall**. Finally, we recall that the insertion of paper layers between the stainless steel sidewall and the fluid results in a significantly less sharp transition. In contrast, two other changes to the sidewall thermal properties (using a thicker wall and modifying the temperature distribution along the wall) only had a limited effect. This result is not understood but reveals that the sidewall plays some role in the transition, as already suggested by the comparison of cells with different aspect ratios.

7. Conclusion

We have presented a systematic study of the convection regime reported in Grenoble in 1996 and then named the Ultimate Regime of convection. In particular, we have characterized the conditions for the triggering of this regime. Among the results, we have shown that all Rayleigh–Bénard experiments conducted at very high Ra using cryogenic helium are consistent if we assume that low Pr tend to disfavour the transition in aspect ratio $\Gamma = 0.5$ cells. We have also found that the LSC present in the cells does not play a key role in triggering the transition, contrary to a common assumption. Conversely, we have found that the sidewall has an unexpected effect on this transition.

Several lines of evidence suggest that Grenoble's regime corresponds to Kraichnan's prediction and no experimental fact seems incompatible with such an interpretation. Nevertheless, the conditions for the triggering of this regime are obscure and sometimes surprising. In addition, a few experimental facts cannot be directly explained using the genuine Kraichnan model. Further experimental investigations are clearly needed.

On the theoretical side, the Kraichnan regime is the only elaborated model available to interpret the Grenoble regime. Alternative scenarios of boundary layer instability probably deserve to be explored, aside from Kraichnan's paradigm or in a complementary fashion. We hope that the results presented in this work will set useful bounds for such alternative models.

Acknowledgments

We thank B Castaing, F Chillà, R Du Puits, B Hébral and B Chabaud for scientific discussions and support. We acknowledge the laboratory cryogenic staff, and in particular G Garde, for providing us with most of the convection cells presented in this work. We do not forget V Arp who kindly shared with us some helium properties fits and the students R Bois, J Muzellier and E Waites who contributed at some point to these investigations.

Appendix. The Grenoble regime and the Boussinesq approximation

We report here two systematic and complementary studies of non-Boussinesq deviations at very high Ra. An experimental study explores the validity of the 'constant fluid properties' approximation [46], while the theoretical study addresses the validity of all the other approximations required to obtain Boussinesq's set of equations [47]. The 'constant fluid properties' approximation in the context of very-high-Ra convection has already been discussed in the literature (e.g. [18, 48]).

A.1. The variation in fluid properties

In given experimental conditions, the variations in the different fluid properties across the cell occur simultaneously. It is therefore convenient to parametrize them with a single parameter. A convenient one is the first-order approximation of the density variation, $\delta\rho/\rho \simeq \alpha\Delta$. A more stringent parameter Υ is the maximum deviation among the five parameters coming into the definition of Ra, Pr and Nu: the density ρ, the thermal expansion α, the molecular conductivity k, the isobaric heat capacity c_p and the viscosity η. In practice, we defined it as $\Upsilon = 2 \cdot \max(|\delta A_{\text{top}}|/A_{\text{top}}, |\delta A_{\text{bottom}}|/A_{\text{bottom}})$, where $A \in \{\rho, \alpha, k, c_p, \eta\}$ and where the indices

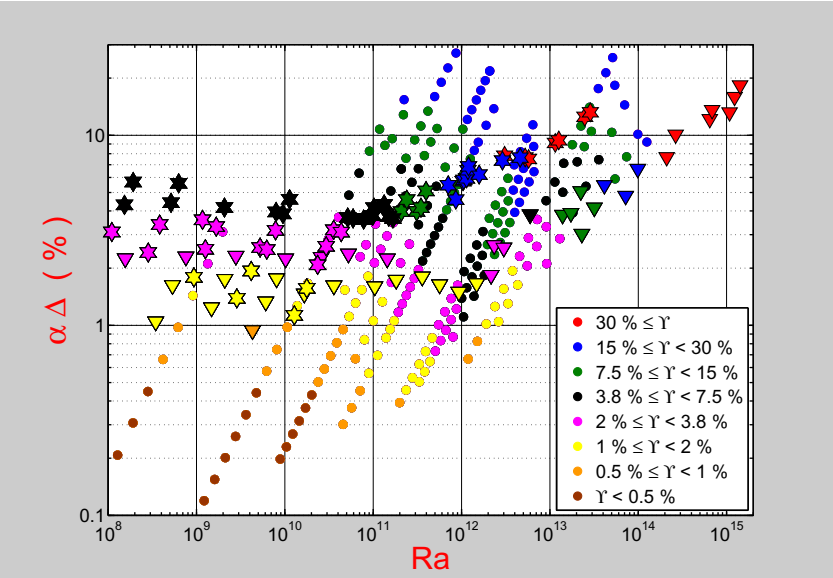

Figure A.1. Non-Boussinesq variation of fluid properties in the *Flange* cell (discs), Oregon (triangles) and Trieste $\Gamma = 1$ (stars) experiments. The non-Boussinesq parameter is defined in the text.

top and bottom represent the 'top' and 'bottom' boundary layers. Using these two non-Boussinesq parameters, we now compare the datasets of the *Flange* cell, Trieste $\Gamma = 1$ and Oregon experiments. Among our cells, the *Flange* cell is chosen because it benefited the most extensively from exploration of the parameter space. All three cells used the same fluid and therefore they are expected to experience somehow a similar variation of fluid properties. We recall that the Oregon cell does not transit at very high Ra, contrary to the other two.

Figure A.1 shows the non-Boussinesq parameters $\alpha\Delta$ (y-axis) and Υ (colour code) for the three experiments. At first, for any given Ra, the non-Boussinesq deviations in the Grenoble 20 cm-high cell can be significantly smaller than the corresponding deviations in the Trieste 50 cm-high cell and at least as good as the 100 cm-high cell of Oregon. This contradicts the widespread idea that larger cells are necessarily 'more' Boussinesq for a given Ra.

More interestingly, for a given Ra, the non-Boussinesq parameter $\alpha\Delta$ of the Grenoble experiment is varied over up to 1.5 decades, reaching values equal to or above the ones reached in the Oregon cell. At $Ra = 2 \times 10^{12}$ (for example), the non-Boussinesq parameters $\alpha\Delta$ and Υ are close to 2% in the Oregon experiment. At the same Ra, these parameters span a range from 1% to nearly 30% in Grenoble's cell. Over all this range of non-Boussinesq parameters, the Grenoble Ultimate regime is present in the Grenoble experiment but not in the Oregon one. This shows that the non-Boussinesq deviations associated with fluid properties variations cannot cause a qualitative difference between these two experiments.

Figure A.2(a) shows the local scaling exponent of $Nu(Ra)$ in the Grenoble cell for two Ra: below and above the transition. Each exponent was fitted manually using the subsets of (Ra, Nu) data obtained at constant mean density and mean temperature. For these two specific Ra, the non-Boussinesq parameter $\alpha\Delta$ varies over more than one decade without causing any noticeable change in scaling exponent. It is worth pointing out that the Grenoble regime is clearly evidenced with a non-Boussinesq parameter $\alpha\Delta$ smaller than 1%.

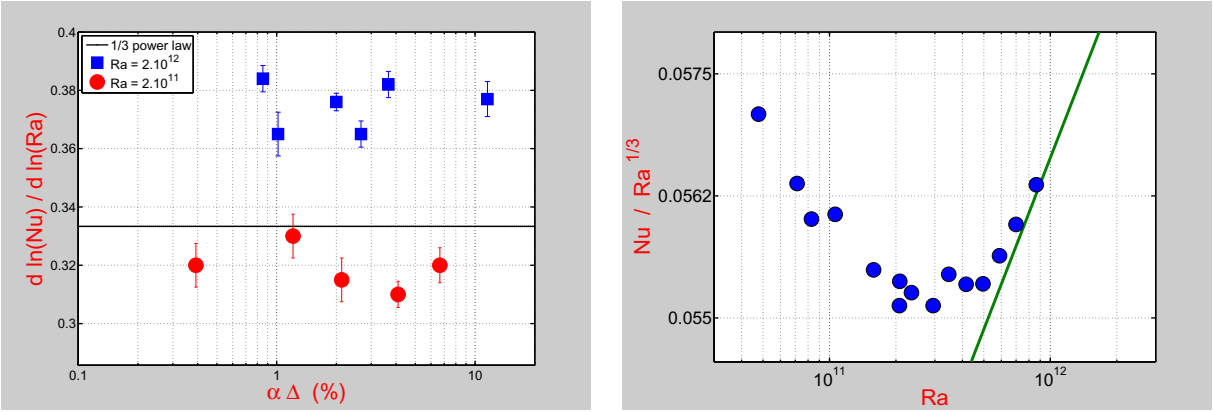

(a) (b)

Figure A.2. (a) Local exponent of the $Nu(Ra)$ dependence versus the non-Boussinesq parameter $\alpha\Delta$. The Rayleigh numbers $Ra = 2 \times 10^{11}$ and 2×10^{12} were chosen on each side of the transition to the Ultimate Regime. (b) Evidence of the transition at a mean density of 18.69 kg m^{-3} and a mean temperature of 11.4 K, that is, at about a quarter of the critical density and at twice the critical temperature.

A.2. Non-Boussinesq deviations without fluid properties variation

Boussinesq's approximation not only consists in neglecting variation in fluid properties and modelling at first order the buoyant term; it also requires a decoupling of the heat balance equation with the flow mechanical energy. For example, the heating produced by viscous dissipation and temperature fluctuations induced by pressure fluctuations are neglected in this approximation. In his famous book [49], D J Tritton discusses in detail the applicability of this approximation at low Ra, where gradient and time derivatives can be estimated using integral length and time scales h and $h^2/\nu Re$. In the turbulent regimes, these gradients could *a priori* become significantly larger due to the smaller characteristic scales and Tritton's criteria are no longer useful. Using the present knowledge of scaling laws in turbulent convection, we derived a set of criteria for the applicability of Boussinesq's approximation in a fluid with constant properties and Pr of order 1–10. Details of the derivation are given in [50]. The result is a set of four criteria,

$$\begin{cases} \alpha\Delta \ll 1, \\ \alpha\Delta_h \times \dfrac{PrRe^2}{Ra\theta^\star_{\mathrm{rms}}} \ll 1, \\ \dfrac{\Delta_h}{T_0} \times \left(\dfrac{Pr^2Re^3}{Ra\theta^\star_{\partial t}} + \dfrac{PrRe}{4Nu^2} \right) \ll 1, \\ \dfrac{\Delta_h^2}{T_0\Delta} \times \dfrac{PrRe}{2\theta^\star_{\partial t}} \ll 1, \end{cases}$$

where $\theta^\star_{\mathrm{rms}}$ is a dimensionless estimation of the temperature fluctuations in the bulk of the flow and $\theta^\star_{\partial t}$ is an estimation of its associated time derivative $\partial\theta/\partial t\,(h^2/\Delta\kappa)$. The adiabatic gradient

Δ_h/h, the compressibility χ, the heat capacities ratio $\gamma = c_p/c_v$ and the mean temperature T_0 are related by

$$\alpha\Delta_h = \alpha^2 g T_0 h/c_p = \rho_0 g \chi h(1-\gamma^{-1}) \sim \rho_0 g \chi h.$$

Physically, the first criterion is required for incompressibility in the boundary layer and it was considered in the first part of this appendix. The second criterion allows one to neglect variations in density due to pressure variations, versus those due to temperature variations. It also allows one to neglect the cooling/heating associated with pressure variations experienced by a fluid particle in the heat transport equation. The two other criteria, indirectly associated with the stratification in the cell, result from various physical contributions. Using fits for Re, Nu, $\theta^\star_{\rm rms}$ and $\theta^\star_{\partial t}$, the above four criteria become

$$\begin{cases} \alpha\Delta \ll 1, \\ (\alpha\Delta_h) \times 0.1 Ra^{0.13} \ll 1, \\ \left(\dfrac{\Delta_h}{T_0}\right) \times \left[\dfrac{Ra^{0.1} Pr^{-0.25} x}{200} + 10 Ra^{-0.17} Pr^{0.25}\right] \ll 1, \\ \left(\dfrac{\Delta_h^2}{T_0\Delta}\right) \times 0.1 Ra^{0.1} Pr^{0.25} \ll 1. \end{cases}$$

Our main interest is to see whether a violation of criterion 2, 3 or 4 is correlated with the occurence/inhibition of the transition to the Grenoble regime. We find that, up to $Ra \simeq 10^{16}$, the Oregon and Grenoble He experiments fulfil the last three criteria provided that the first one is fulfilled [50][5]. As a conclusion, the type of non-Boussinesq deviation considered in this subsection cannot explain the puzzle at very high Ra.

A.3. A critical point effect?

The convection literature repeatedly states that the cryogenic He experiments are performed 'close to the critical point' and suggests that some unknown critical point artifacts could somehow alter heat transfer measurements at very high Ra.

Firstly, we note that no precise statement along this line has ever been published.

Secondly, this hypothesis has been discussed in [48] comparing the datasets of Chavanne *et al* [2], Oregon [16] and Chicago [4]. The conclusion was that proximity to the liquid–vapour coexistence curve cannot cause a difference in heat transfer.

A third argument can be raised using the *Flange* cell datasets. The 'distance' to the critical point (T_c, ρ_c) can be assessed quantitatively using the reduced temperature $|T - T_c|/T_c$ and the reduced density $|\rho - \rho_c|/\rho_c$. It is well known that critical point divergence phenomena become significant when both reduced parameters are significantly smaller than unity. In [15], for example, the reduced temperature is made smaller than 10^{-2} to experience the compressibility effect. On the other hand, the reduced temperature and density of water in traditional convection experiments are about 0.5 and 2, respectively, and one can safely consider these experiments as far away from the critical point. For $Ra = 10^{13}$, the reduced density in the Oregon cell is

[5] Above $Ra \simeq 10^{16}$, criterion 2 is violated in the Oregon experiment. A side consequence is that increasing the height of the He cell beyond 1 m will only allow one to increase the maximum Ra (within Boussinesq conditions) like h^2 and not h^3.

about 0.9 (that is, $\rho \simeq \rho_c/10$): undoubtedly a critical point artifact cannot explain the absence of transition in this cell. In the Grenoble *Flange* cell, the transition was evidenced for reduced temperatures up to 1.2 ($T \simeq 2.2\,T_c$) and a reduced density close to 0.7 ($\rho \simeq \rho_c/3.7$), as shown in figure A.2(b). The occurrence of the transition cannot be seriously attributed to a critical point artifact.

As a conclusion, it seems very unlikely that any sort of non-Boussinesq deviation could explain the apparent scatter of heat transfer measurements at very high Ra.

References

Q1

[1] Chavanne X, Chillà F, Chabaud B, Castaing B, Chaussy J and Hébral B 1996 High Rayleigh number convection with gaseous helium at low temperature *J. Low Temp. Phys.* **104** 109–29

[2] Chavanne X, Chillà F, Castaing B, Hébral B, Chabaud B and Chaussy J 1997 Observation of the ultimate regime in Rayleigh-Bénard convection *Phys. Rev. Lett.* **79** 3648–51

[3] Kraichnan R 1992 Turbulent thermal convection at arbitrary Prandtl numbers *Phys. Fluids* **5** 1374

[4] Wu X-Z 1991 Along a road to developed turbulence: free thermal convection in low temperature helium gas *PhD Thesis* University of Chicago

[5] Sommeria J 1999 The elusive 'ultimate state' of thermal convection *Nature* **398** 294

[6] Roche P-E, Castaing B, Chabaud B and Hébral B 2004 Heat transfer in turbulent Rayleigh–Bénard convection below the ultimate regime *J. Low Temp. Phys.* **134** 1011–42

[7] Ahlers G, Grossmann S and Lohse D 2009 Heat transfer and large scale dynamics in turbulent Rayleigh–Bénard convection *Rev. Mod. Phys.* **81** 503–37

[8] Lohse D and Toschi F 2003 Ultimate state of thermal convection *Phys. Rev. Lett.* **90** 034502

[9] Chavanne X, Chillà F, Chabaud B, Castaing B and Hébral B 2001 Turbulent Rayleigh–Bénard convection in gaseous and liquid He *Phys. Fluids* **13** 1300–20

[10] Gauthier F and Roche P-E 2008 Evidence of a boundary layer instability at very high Rayleigh number *Europhys. Lett.* **83** 24005

[11] Roche P-E, Castaing B, Chabaud B and Hébral B 2001 Observation of the 1/2 power law in Rayleigh–Bénard convection *Phys. Rev.* E **63** 045303

[12] Roche P-E, Gauthier F, Chabaud B and Hébral B 2005 Ultimate regime of convection: robustness to poor thermal reservoirs *Phys. Fluids* **17** 115107

[13] Salort J, Gauthier F, Chabaud B, Bourgeois O, Garden J-L, du Puits R, Thess A and Roche P-E 2009 Convection at very high Rayleigh number: signature of transition from a micro-thermometer inside the flow *Advances in Turbulence XII: Proc. 12th EUROMECH European Turbulence Conf. (Springer Proc. in Physics vol 132)* (Marburg, Germany 7–10 Sept. 2009) pp 159–62 ed B Eckhardt (Berlin and Heidelberg: Springer)

[14] Gauthier F, Hébral B, Muzellier J and Roche P-E 2007 Ultimate regime of convection: search for a hidden triggering parameter *Advances in Turbulence XI, (Springer Proc. in Physics)* vol 117 ed J M L M Palma and A Silva Lopes (Heidelberg: Springer) pp 645

[15] Ashkenazi S and Steinberg V 1999 High Rayleigh number turbulent convection in a gas near the gas–liquid critical point *Phys. Rev. Lett.* **83** 3641–4

Burnishev Y, Segre E and Steinberg V 2010 Strong symmetrical non-Oberbeck–Boussinesq turbulent convection and the role of compressibility *Phys. Fluids* **22** 035108

[16] Niemela J J, Skrbek L, Sreenivasan K R and Donnelly R J 2000 Turbulent convection at very high Rayleigh numbers *Nature* **404** 837–40

[17] Niemela J J and Sreenivasan K R 2003 Confined turbulent convection *J. Fluid Mech.* **481** 355–84

[18] Niemela J J and Sreenivasan K R 2006 Turbulent convection at high Rayleigh numbers and aspect ratio 4 *J. Fluid Mech.* **557** 411–22

[19] Ahlers G, Funfschilling D and Bodenschatz E 2009 Transitions in heat transport by turbulent convection at Rayleigh numbers up to 1e15 *New J. Phys.* **11** 123001
[20] Kenjereš S and Hanjalić K 2002 Numerical insight into flow structure in ultraturbulent thermal convection *Phys. Rev.* E **66** 036307
[21] Roche P-E, Castaing B, Chabaud B, Hébral B and Sommeria J 2001 Side wall effects in Rayleigh–Bénard experiments *Eur. Phys. J.* B **24** 405–8
[22] Verzicco R 2002 Side wall finite conductivity effects in confined turbulent thermal convection *J. Fluid Mech.* **473** 201–10
[23] Verzicco R 2003 Effects of nonperfect thermal sources in turbulent thermal convection *Phys. Fluids* **16** 1965
[24] Roche P-E, Castaing B, Chabaud B and Hébral B 2002 Prandtl and Rayleigh numbers dependences in Rayleigh–Bénard convection *Europhys. Lett.* **58** 693–8
[25] Chaumat S, Castaing B and Chillà F 2002 Rayleigh–Bénard cells: influence of the plate properties *Advances in Turbulence IX, Proc. 9th European Turbulence Conf. (Southampton, UK 2–5 July 2002)* ed I P Castro and P E Hancock (Barcelona: CIMNE) pp 159–62
[26] Krishnamurti R and Howard L N 1981 Large-scale flow generation in turbulent convection *Proc. Natl Acad. Sci. USA* **78** 1981–5
[27] Roche P-E 2001 *Convection thermique turbulente en cellule de Rayleigh–Bénard cryogénique PhD Thesis* Université Joseph-Fourier
[28] Mitin V F *et al* 2007 Ge-on-GaAs film resistance thermometers for cryogenic applications *Cryogenics* **47** 474–82
[29] Lam S, Shang X D, Zhou S Q and Xia K-Q 2002 Prandtl number dependence of the viscous boundary layer and the Reynolds numbers in Rayleigh–Bénard convection *Phys. Rev.* E **65** 066306
[30] Sun C and Xia K-Q 2005 Scaling of the Reynolds number on turbulent thermal convection *Phys. Rev.* E **72** 067302
[31] Brown E and Ahlers G 2007 Large-scale circulation model for turbulent Rayleigh-Bénard convection *Phys. Rev. Lett.* **98** 134501
[32] Niemela J J and Sreenivasan K R 2003 Rayleigh-number evolution of large-scale coherent motion in turbulent convection *Europhys. Lett.* **62** 829–33
[33] Niemela J J, Skrbek L, Sreenivasan K R and Donnelly R J 2001 The wind in confined thermal convection *J. Fluid Mech.* **449** 169–78
[34] Brown E and Ahlers G 2006 Rotations and cessations of the large-scale circulation in turbulent Rayleigh–Bénard convection *J. Fluid Mech.* **568** 351–86
[35] Xi H-D and Xia K-Q 2008 Flow mode transitions in turbulent thermal convection *Phys. Fluids* **20** 055104
[36] Chillà F, Rastello M, Chaumat S and Castaing B 2004 Long relaxation times and tilt sensitivity in Rayleigh–Bénard turbulence *Eur. Phys. J.* B **40** 223–7
[37] Sun C, Xi H-D and Xia K-Q 2005 Azimuthal symmetry, flow dynamics and heat transport in turbulent thermal convection in a cylinder with an aspect ratio of 0.5 *Phys. Rev. Lett.* **95** 074502
[38] Ciliberto S, Cioni S and Laroche C 1996 Large-scale flow properties of turbulent thermal convection *Phys. Rev.* E **54** R5901–4
[39] Xia K-Q and Lui S-L 1997 Turbulent thermal convection with an obstructed sidewall *Phys. Rev. Lett.* **79** 5006
[40] Verzicco R and Camussi R 2003 Numerical experiments on strongly turbulent thermal convection in a slender cylindrical cell *J. Fluid Mech.* **477** 19–49
[41] Grossmann S and Lohse D 2002 Prandtl and Rayleigh number dependence of the Reynolds number in turbulent thermal convection *Phys. Rev.* E **66** 016305
[42] Gauthier F, Salort J, Bourgeois O, Garden J-L, Du Puits R, Thess A and Roche P-E 2009 Transition on local temperature fluctuations in highly turbulent convection *Europhys. Lett.* **87** 44006
[43] Belmonte A, Tilgner A and Libchaber A 1993 Boundary layer length scales in thermal turbulence *Phys. Rev. Lett.* **70** 4067
[44] Sun C, Cheung Y-H and Xia K-Q 2008 Experimental studies of the viscous boundary layer properties in turbulent Rayleigh–Bénard convection *J. Fluid Mech.* **605** 79–113

[45] Malkus W V R 1954 The heat transport and spectrum of thermal turbulence *Proc. Roy. Soc.* A **225** 196–212
[46] Oberbeck A 1879 Ueber die wärmeleitung der flüssigkeiten bei berücksichtigung der strömungen infolge von temperaturdifferenzen *Ann. Phys. Chem.* **VII** 271–92
[47] Boussinesq J 1903 *Théorie analytique de la chaleur* (Paris: Gauthier-Villars) http://gallica.bnf.fr/ark:/12148/bpt6k5529353q.f6.langEN
[48] Chavanne X, Roche P-E, Chabaud B, Hébral B, Chillà F and Castaing B 2006 Comment on 'Turbulent heat transport near critical points: non-Boussinesq effects' arXiv:cond-mat:0603262
[49] Tritton D J 1988 *Physical Fluid Dynamics* (Oxford: Clarendon) 2nd ed
[50] Roche P-E 2007 Applicability of Boussinesq approximation in a turbulent fluid with constant properties arXiv:0710.3497